Fractal Representation of Turbulent Dispersing Plumes

R. I. SYKES AND R. S. GABRUK

ARAP Group, California Research and Technology Division, Titan Corporation, Princeton, New Jersey

(Manuscript received 5 May 1993, in final form 17 November 1993)

ABSTRACT

Fractal analysis techniques have been applied to the concentration fields from large-eddy simulations of plume dispersion in a turbulent boundary layer. Fractal dimensions between 1.3 and 1.35 are obtained from area–perimeter and box-counting analyses for neutral and convective conditions. These values are close to previous estimates from atmospheric data. Methods for generating fractal fields with given statistical moments are examined and the simplest of these, the recursive refinement technique, is shown to be inadequate. The problem is shown to be the interpolation step of the procedure, which intrinsically reduces the variance with each refinement. Accurate statistical representation is obtained by replacing the interpolation step of the refinement technique with a sum of random pulses of appropriate width and random location. The pulse technique can easily be adapted to generate either clipped-normal or lognormal one-point probability distributions. Results from the fractal generation technique using simulated mean statistics are compared with realizations of instantaneous plume cross sections from the large-eddy simulations. The simulated probability distributions lie between the clipped normal and the lognormal, so the fractal fields cannot match the realizations precisely. Larger-scale features of the plumes are generally well represented by the fractal method, however.

1. Introduction

Turbulent dispersion of a contaminant in the planetary boundary layer is a chaotic process. The instantaneous concentration field exhibits variations on a range of length and timescales, corresponding to the spectrum of motions in the turbulent velocity field. This random character of tracer dispersion has been recognized by atmospheric modelers and has lead to explicit statistical descriptions of the concentration variable. There has been extensive research on characterizing the small-scale fluctuations in the concentration field, both experimentally in the laboratory (Fackrell and Robins 1982) and observationally in the atmosphere (Lewellen and Sykes 1986; Sawford 1987; Mylne and Mason 1991). These studies have been supported by modeling efforts (Durbin 1980; Kaplan and Dinar 1988; Sykes et al. 1984) and considerable progress has been made in our understanding of the fluctuation statistics.

For model evaluation applications, where it is important to characterize the variability in a sampler observation, one-point statistics are usually sufficient. Most tracer measurements involve a time average at a fixed location. There are other situations where more detailed information about the spatial and temporal structure of the plume is required, however. For example, any system with a nonlinear response to the concentration level needs more statistical information to predict the integrated response from passage through the plume. Such response systems might include human health effects and toxicity, or visibility and optical propagation phenomena. A realistic representation of the complete concentration distribution is useful for the assessment of parameterized effects models.

As a preliminary step toward a general description, we examine some simple fractal field generation methods to determine their consistency with known plume characteristics. Fractal geometry has been used to analyze turbulent fields in several contexts (Sreenivasan and Meneveau 1986; Prasad and Sreenivasan 1990a,b; Lovejoy and Mandelbrot 1985) and provides a natural method for describing the self-similar nature of the turbulent cascade process. Multifractal cascade models have also been successfully applied to the study of turbulent flow fields (e.g., Prasad et al. 1988; Sreenivasan 1991), but the mathematical definition of multifractal properties in terms of the structure of the field singularities (Lovejoy and Schertzer 1991) is most appropriate for highly intermittent fields such as energy dissipation or scalar fluctuation dissipation. Scalar concentration fields do not exhibit singularities and are generally described in terms of a simple fractal isosurface dimension (Sreenivasan 1991; Lane-Serff 1993). The characterization of scalar isosurfaces in terms of monofractal properties is imperfect but is a reasonable step toward a more general approach.

Corresponding author address: Dr. R. Ian Sykes, A.R.A.P. Group, California Research and Technology Division, 50 Washington Road, P.O. Box 2229, Princeton, NJ 08543-2229.

© 1994 American Meteorological Society

Unauthenticated | Downloaded 05/25/22 11:18 PM UTC

Fractal fields can be generated with the appropriate degree of complexity and spatial structure and can be used to produce "cloudlike" fields (Lovejoy and Mandelbrot 1985). Our objective here is not simply to produce a visual image reminiscent of a dispersing plume, but rather to generate a "realization" that is statistically consistent with a given plume and can therefore be used for quantitative analysis. We note, however, that simple fractal representations cannot necessarily reproduce the large-scale "coherent structures" in a flow field (Sreenivasan and Meneveau 1986), since the large-scale structures are generally determined by the mean flow geometry and do not exhibit self-similar structure.

The principal data source for the fractal parameters is the LES (large-eddy simulation) plume calculations of Sykes and Henn (1992) and Henn and Sykes (1992). These explicit numerical calculations of the time-dependent, three-dimensional plume dispersion have provided a number of "realizations" of the instantaneous plume. The numerical results have previously been analyzed to obtain statistical measures such as concentration moments, spatial and temporal correlations, and one-point probability distribution functions, and these parameters will be required for a fractal generation scheme. In this paper, we shall present fractal dimension analyses of the concentration fields in order to quantify a fractal description of the LES plumes.

Given the statistical plume parameters, we examine techniques for generating a fractal field with the correct ensemble mean and variance values. We present a simple method for producing a random realization with either a "clipped-normal" probability distribution (Lewellen and Sykes 1986) or a lognormal distribution. Finally, we compare the characteristics of the fractal-generated plume cross sections with the LES realizations.

2. Fractal analysis of the LES plumes

A detailed description of the numerical methodology employed in the LES calculations is given by Sykes and Henn (1992). Simulations were performed for a neutral, wind tunnel boundary layer and for a free-convection layer driven by a surface buoyancy flux. Dispersion from elevated releases of a passive scalar was calculated for each flow, and the evolving plume was computed for several boundary-layer heights downstream. A uniform translation velocity was imposed on the free-convection layer to produce a statistically steady plume.

The fractal analysis of the neutral and free-convection boundary layers was performed with both area–perimeter and box-counting analyses. Area–perimeter analysis, a method for estimating the fractal dimension of planar shapes, was first proposed by Mandelbrot (1977) and is the method used by Lovejoy (1982) in his investigation of satellite and radar pictures of rain and cloud areas. The area–perimeter relationship determines the complexity of the boundary of a shape since a very convoluted perimeter will be longer than a smooth one for the same enclosed area. The fractal dimension D characterizes the degree of contortion of the boundary and is obtained from the relation $P \propto A^{D/2}$, where P is the perimeter and A is the area. A reasonable estimate of D requires a dataset of area–perimeter pairs covering sufficient range for the exponent to be reliably determined. Lovejoy and Schertzer (1991) showed that the area–perimeter relation in its original form (given above) can be used only when nonfractal areas are enclosed by fractal perimeters.

In Lovejoy's analysis (1982) of rain and cloud areas, a large database of satellite and radar pictures supplied the necessary information over a wide range of scales. For the LES plumes used in the current research, however, the range of cloud (plume) sizes was somewhat limited. In order to extend the range of sizes, cross sections of the plume were taken at locations ranging from 0.83 to 6.67 boundary-layer heights downstream of the source for the neutral case and from 1 to 8 boundary-layer heights for the convective case. Lovejoy showed that when the threshold on the satellite data of his study was varied, the sizes of the clouds changed, but the perimeters changed in the same self-similar manner. Therefore, in order to further extend the range of sizes, the threshold value defining the plume boundary was varied. Multiple independent realizations of each plume (eight for the neutral and six for the convective) were analyzed to improve statistical confidence in the power-law relationship.

Box counting, a recursive technique for estimating the fractal dimension of a set, is described by both Mandelbrot (1982) and Feder (1988), and is employed by Malinowski and Zawadzki (1993) in their recent analysis of cloud surfaces. Similar approaches were used by Sreenivasan and Meneveau (1986) and Sreenivasan (1991) in their research on turbulent flows. The box-counting method utilizes a grid of rectangular boxes to cover the space occupied by a set, and counts the number of boxes needed to completely cover the set itself. This number will depend on the size of the covering boxes. If the number varies in proportion to a power of the box size, the exponent is called the box dimension of the set (Feder 1988). The estimate of the box dimension can vary slightly due to the uncertainty in the placement of a given grid since a slight shift in grid location may change the number of boxes counted. Therefore, in order to obtain a better approximation of the fractal dimension of the set, the grid location was shifted on each level and the number of boxes counted was averaged. Edge effects due to

Unauthenticated | Downloaded 05/25/22 11:18 PM UTC

dataset truncation were avoided by only counting boxes centered within the range of data.

The datasets chosen for box-counting analysis were isoconcentration contours obtained from vertical transverse slices of the LES plumes. LES calculations were performed on grids of 240 × 90 for the neutral boundary layer and 80 × 50 for the convective layer. Figure 1 shows typical contours for the neutral and convective boundary layers. In Fig. 1, $\bar{c}_m$ is the maximum mean concentration obtained from multiple realizations of the concentration field. Although the contour level is somewhat arbitrary, the chosen values fell within a range of concentrations ($0.003 < c/\bar{c}_m < 0.3$) that produced approximately the same fractal dimension (±0.05). The concentration value must be small enough to give an extensive contour but not so small that numerical errors are significant. The locations of the plume slices were 5 and 8 boundary-layer heights downstream of the source for the neutral and convective layers, respectively. For the convective layer, z_i denotes the mixed-layer depth, while H is the depth of the neutral layer (Sykes and Henn 1992). Results of the area–perimeter and box-counting analyses for the neutral and free-convection boundary layers are shown in Figs. 2 and 3, respectively.

Both Figs. 2a and 2b display approximately linear sections over most of the plot range. Since these two plots are on log–log scales, the linear sections indicate power-law relations between the abscissa and ordinate variables. For the area–perimeter analysis, the relation

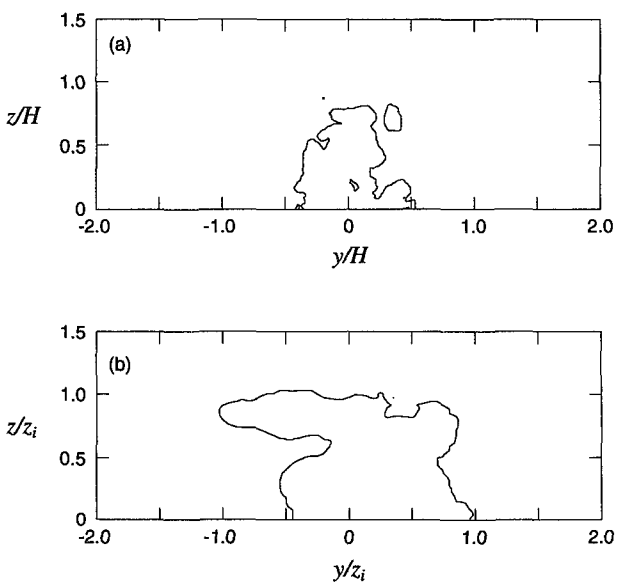

FIG. 1. Transverse cross section of instantaneous isoconcentration contours from high-resolution LES fields with $c/\bar{c}_m = 0.01$, where $\bar{c}_m$ is the maximum mean concentration over multiple realizations. (a) Neutral boundary layer at $x/H = 5$. (b) Convective boundary layer at $x/z_i = 8$.

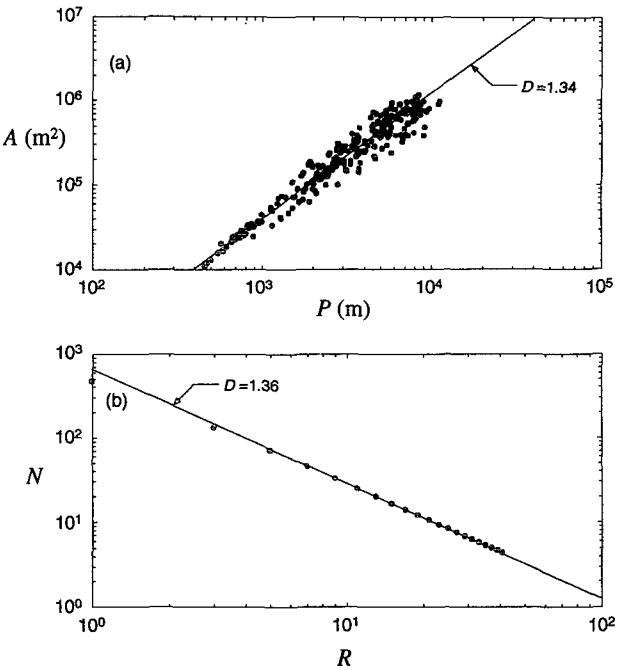

FIG. 2. Fractal analyses of neutral boundary layer. (a) Area–perimeter analysis; P is perimeter in meters and A is area in square meters. (b) Box-counting analysis; R is normalized box size and N is the number of boxes counted.

$P \propto A^{D/2}$ is used to determine the fractal dimension D of the plume boundary by a least-squares regression of the dataset. The areas of the plume cross sections were determined to be nonfractal, thus legitimizing the use of the area–perimeter relation for determination of the fractal dimension of the perimeter. The box dimension is also determined from a regression line fit through the box-counting results. For the neutral boundary layer (Fig. 2), the box dimension is 1.34 in the area–perimeter analysis and 1.36 in the box-counting analysis. Results from the free-convection boundary layer (Fig. 3) indicate a fractal dimension of 1.32 using both methods. These fractal dimensions all had uncertainties of about ±0.05.

A direct comparison between the results of the LES fractal analyses and those of other atmospheric fractal studies is not a simple task. Most previous fractal analyses have utilized cloud radiances (obtained by radar or satellite) and not cloud densities (as in this study). There is no simple one-to-one correspondence between radiance and density, according to Cahalan and Joseph (1989). However, the lack of results pertaining to cloud densities necessitates comparisons between density and radiance results with the understanding that there is not necessarily a simple relationship between the two.

Although the datasets studied here are neither rain nor cloud areas, it is reasonable to compare the results with those of cloud areas since both are being shaped

Unauthenticated | Downloaded 05/25/22 11:18 PM UTC

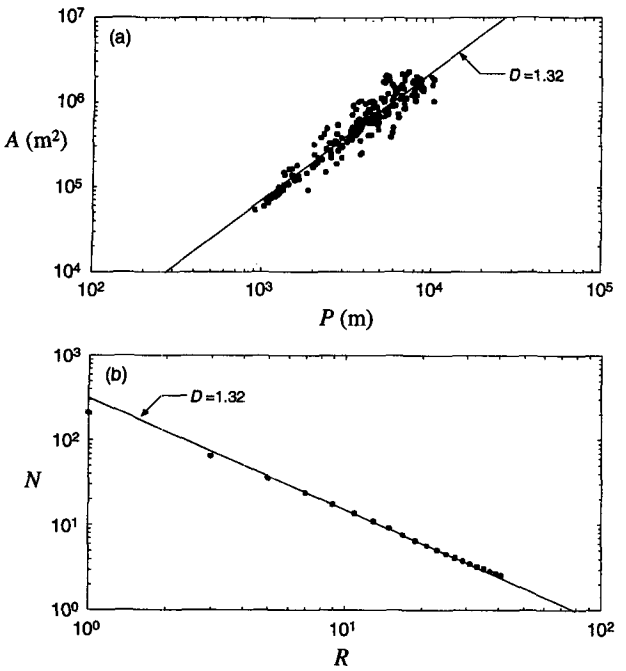

FIG. 3. Fractal analyses of convective boundary layer. (a) Area–perimeter analysis; P is perimeter in meters and A is area in square meters. (b) Box-counting analysis; R is normalized box size and N is the number of boxes counted.

by the ambient turbulence of the atmosphere. The results of the present study are consistent with those of Lovejoy (1982), who found (using the perimeter–area relation on cloud radiances) the cloud perimeter fractal dimension to be 1.35 ± 0.05. Rys and Waldvogel (1986) also used area–perimeter analysis; however, their dataset was radar echo data of severe convective storms. They determined that the fractal dimension of large clouds was 1.36 ± 0.1 and for smaller clouds ($P^{1/D} < 3$ km) was 1.0 ± 0.04. The low dimension for the smaller clouds was believed to be due to strong vertical winds found in thunderstorms. Furthermore, Prasad and Sreenivasan (1990b) estimated a dimension of 1.36 for typical cumulus clouds from box-counting analysis of cloud boundaries in ground-based photographs. Malinowski and Zawadzki (1993), however, report a much higher value of 1.55 from one-dimensional horizontal sections through small cumulus clouds, but this is a different fractal measure and is not necessarily comparable with the planar section perimeter dimension reported here.

In addition to fractal studies on cloud data, other laboratory and analytical results have been published. Prasad and Sreenivasan (1990b) used the box-counting method to analyze images of jet sections (produced from laser-induced fluorescence techniques) and determined that the fractal dimension of jet boundaries was 1.36. Over a wide range, this value was independent of the threshold defining the boundary. In addition, based on the relative turbulent diffusion theory, Hentschel and Procaccia (1984) predicted a slightly higher cloud perimeter fractal dimension in the range between 1.37 and 1.41.

3. Fractal generation technique

The most basic fractal field generation method uses recursive grid refinement with a random addition at each level of iteration (Peitgen and Sauper 1988). In one dimension, random values are generated on an initial coarse grid of size Δ_0. The random numbers are selected from a Gaussian distribution with zero mean and standard deviation σ_0. The refinement process interpolates the initial values onto a finer grid with size $\Delta_1 = \Delta_0/2$, and then adds a random number to every point in the new grid from a distribution with standard deviation σ_1. The fractal dimension of the resulting field is controlled by the specification of $\sigma_1 = \sigma_0 2^{-\alpha}$. The process can be repeated to give a field on a grid of size $\Delta_n = 2^{-n}\Delta_0$, using a standard deviation of $\sigma_n = 2^{-n\alpha}\sigma_0$ to generate the random numbers at that level. The process is illustrated schematically in Fig. 4, and yields a fractal dimension of $D = 2 - \alpha$ for an isosurface in two dimensions.

In considering the recursive refinement technique for the representation of a scalar plume, we must remember that the concentration distribution is nonnegative. This can be achieved in two very simple ways. We can either truncate the field after generation, that is, reset all negative values to zero, or we can generate the logarithm of the concentration. If we use a Gaussian probability distribution for the random numbers at each iteration level in the recursive generation, then the final sum will also have a Gaussian distribution. Thus, truncation of the negative values will produce a clipped-normal distribution, while generation of $\ln c$ (where c is the concentration value) will give a log-normal distribution. The recursive refinement tech-

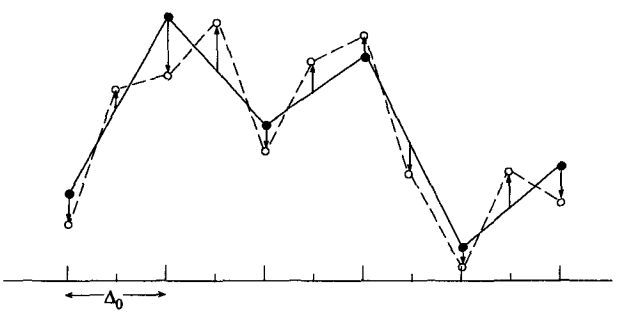

FIG. 4. Schematic illustration of recursive refinement. Points on initial grid shown as solid circles with linear interpolation as solid line. First refinement shown as open circles with random displacement from first-level function.

Unauthenticated | Downloaded 05/25/22 11:18 PM UTC

nique can thus be used to produce fields with two of the most commonly used probability distributions. It should be noted that atmospheric observations (Sawford 1987) as well as the LES calculations show that the concentration pdf (probability distribution function) is more complex than either of the above distributions, but both are valuable representations in appropriate regimes.

The transformation of the Gaussian pdf into the clipped-normal or lognormal pdf by this simple technique does not affect the fractal properties of an isosurface. Our analysis of the fractal nature of the scalar field has considered only scalar isosurfaces, so we must consider the effect of the transformation on these level surfaces. The method can be described as a two-step process; first an untransformed scalar field, g, is generated, and then the desired concentration field is defined as $c = F(g)$. The nonlinear function F represents either truncation or exponentiation for the two distributions described above. A level surface of c is defined as the set of points, $\mathbf{x}$, where $c(\mathbf{x}) = c_0$, say. If F is monotonic, then a unique value g_0 exists such that $F(g_0) = c_0$, provided c_0 is a realizable value—that is, it lies within the range of F. Then the isosurface $c = c_0$ is identical to the level surface $g = g_0$; that is, it is the same set of spatial points. The fractal properties are then obviously identical. The two transform functions utilized in our generation scheme are both monotonic, so we preserve the isosurface fractal properties of the Gaussian field.

In order to test the generation scheme, we consider a one-dimensional, homogeneous field $c(x)$ with unit mean and variance σ_c^2. We generate a periodic field on a domain of length L using an initial grid size Δ_0. The clipped-normal Gaussian parameters (μ_G, σ_G) are defined so that the pdf,

$$p(c) = \gamma\delta(c) + \frac{1}{\sigma_G(2\pi)^{1/2}} \exp\left[\frac{-(c-\mu_G)^2}{2\sigma_G^2}\right], \quad c \geqslant 0 \quad (1)$$

has unit mean and variance σ_c^2. The intermittency γ is defined as

$$\gamma = \frac{1}{2}\left[1 - \text{erf}\left(\frac{\mu_G}{\sigma_G 2^{1/2}}\right)\right] \quad (2)$$

(Lewellen and Sykes 1986). Similarly, the lognormal parameters (μ_l, σ_l) defined as

$$\mu_l = -\frac{1}{2}\ln(1+\sigma_c^2) \quad (3)$$

$$\sigma_l^2 = \ln(1+\sigma_c^2), \quad (4)$$

so that

$$p(x) = \frac{1}{\sigma_l(2\pi)^{1/2}} \exp\left[-\frac{(x-\mu_l)}{2\sigma_l^2}\right], \quad (5)$$

where $x = \ln c$ (Csanady 1973). In the rest of this discussion, we use the clipped-normal parameters to be specific, but all results apply similarly for the lognormal distribution.

The initial variance σ_0^2 for the recursive iteration must be chosen to produce the required variance σ_G^2. Since the random additions are independent, the final variance after N iterations is the sum of the geometric series, so that

$$\sigma_G^2 = \sigma_0^2 \sum_{r=0}^{N} 2^{-2r\alpha} = \sigma_0^2 \frac{1 - 2^{-2(N+1)\alpha}}{1 - 2^{-2\alpha}} \quad (6)$$

for N refinements of the original grid.

The mean concentration value is obtained by specifying μ_G as an initial value for the iteration on the coarse grid. This will be preserved through the random additions since they all have zero mean. The final result for $c(x)$ is obtained by truncating the random field at $c = 0$.

Results from this scheme are illustrated in Fig. 5 for 10 refinements on a unit domain; that is, $L = 1$ and $\Delta_0 = 0.25$. The results are shown for $\sigma_c = 0.25$, with mean statistics from 1000 realizations of the fractal field and $\alpha = 0.7$. The realization shown in the figure is typical of the set. The ensemble mean is close to unity, as required, but the variance shows distinct nonuniformity across the domain.

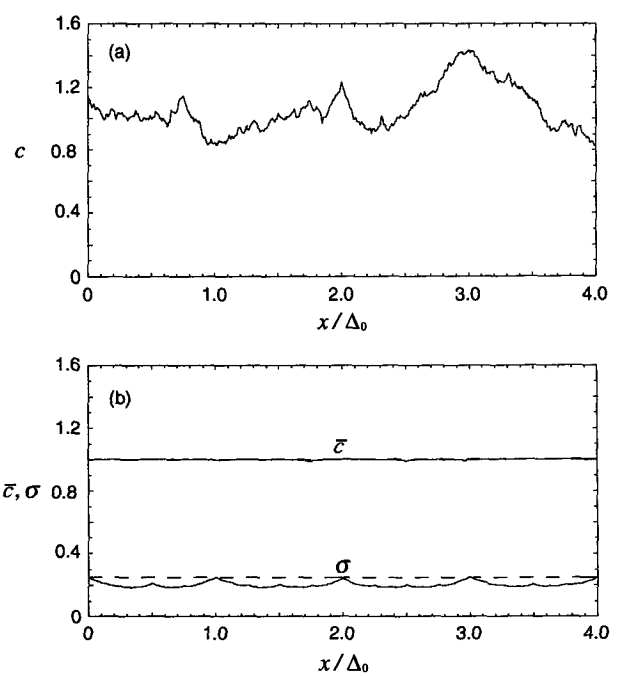

FIG. 5. One-dimensional recursive refinement fractal generation for a homogeneous concentration field with $\sigma_c/\bar{c} = 0.25$. Solid lines are from fractal generation and dashed lines are the target statistics. (a) Individual realization. (b) Mean $\bar{c}$ and rms fluctuation concentration σ from 1000 realizations.

Unauthenticated | Downloaded 05/25/22 11:18 PM UTC

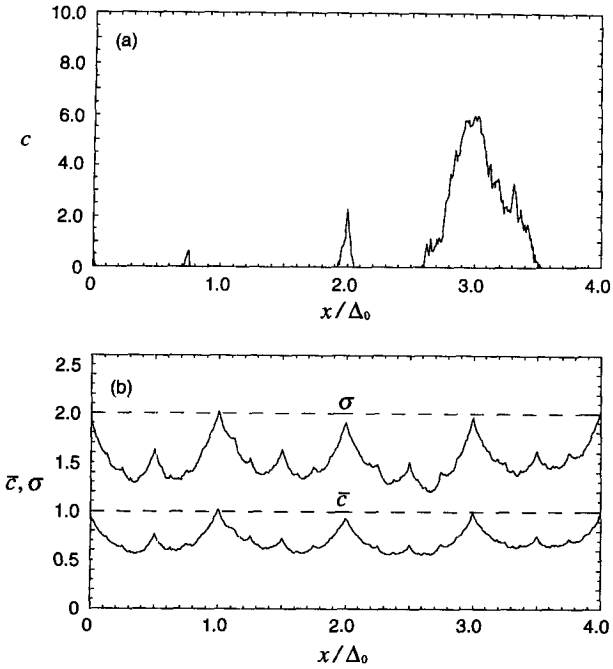

FIG. 6. One-dimensional recursive refinement fractal generation for a homogeneous concentration field with $\sigma_c/\bar{c} = 2$. Solid lines are from fractal generation and dashed lines are the target statistics. (a) Individual realization. (b) Mean $\bar{c}$ and rms fluctuation concentration σ from 1000 realizations.

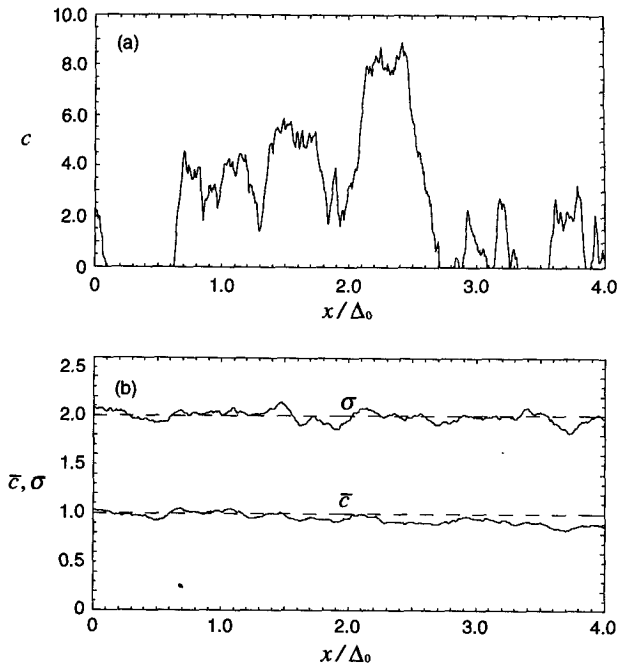

FIG. 7. One-dimensional random pulse fractal generation for a homogeneous concentration field with $\sigma_c/\bar{c} = 2$. Solid lines are from fractal generation and dashed lines are the target statistics. (a) Individual realization. (b) Mean $\bar{c}$ and rms fluctuation concentration σ from 1000 realizations.

The problem with the variance is easily traceable to the interpolation step in the iteration. The geometric sum (6) is valid only on the initial grid. Intermediate points all involve an interpolation between random values, which necessarily reduces the variance. The reduction is evident in the complex pattern of the variance, which shows increasing errors on finer grid locations. The initial coarse grid points are isolated points with the correct variance.

It might be argued that the variance error is not important since the location of the initial grid can be randomly selected to produce a homogeneous ensemble variance. This ensemble average will be smaller than σ_c^2, however. Furthermore, the mean value also shows errors, as illustrated in Fig. 6, when σ_c is larger. Here, $\sigma_c = 2$ and the realization shows the highly intermittent nature of the concentration field. The reduction in the variance prior to the truncation affects the ensemble mean value here, as can be seen from (1). If σ_G is reduced while μ_G remains fixed at some negative value, then the probabilities of zero concentration will increase and the mean and variance will decrease. In this case, randomizing the location of the initial grid will produce an erroneous ensemble-mean value.

The origin of the homogeneity problem is the choice of the initial grid and subsequent interpolation onto the finer grid. We can incorporate the "sum of pulses" concepts of Lovejoy and Mandelbrot (1985) to ran-

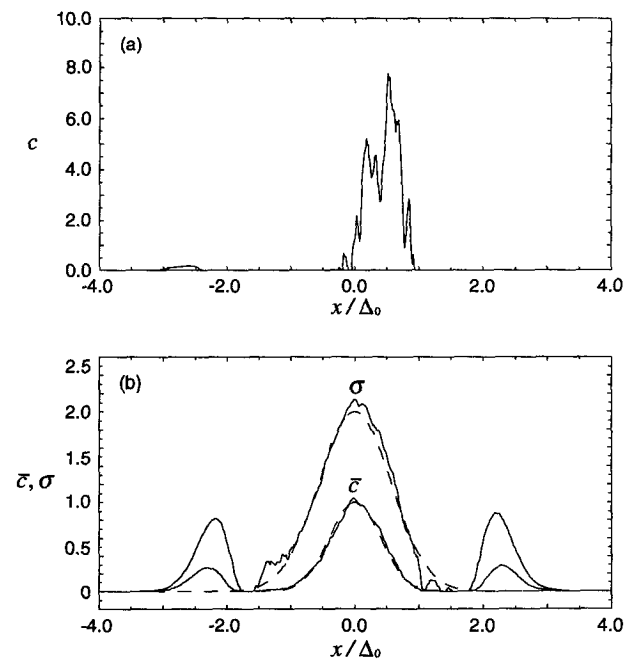

FIG. 8. One-dimensional random pulse fractal generation for an inhomogeneous concentration field with $\sigma_c/\bar{c} = 2$ and no local scaling. Solid lines are from fractal generation and dashed lines are the target statistics. (a) Individual realization. (b) Mean $\bar{c}$ and rms fluctuation concentration σ from 1000 realizations.

Unauthenticated | Downloaded 05/25/22 11:18 PM UTC

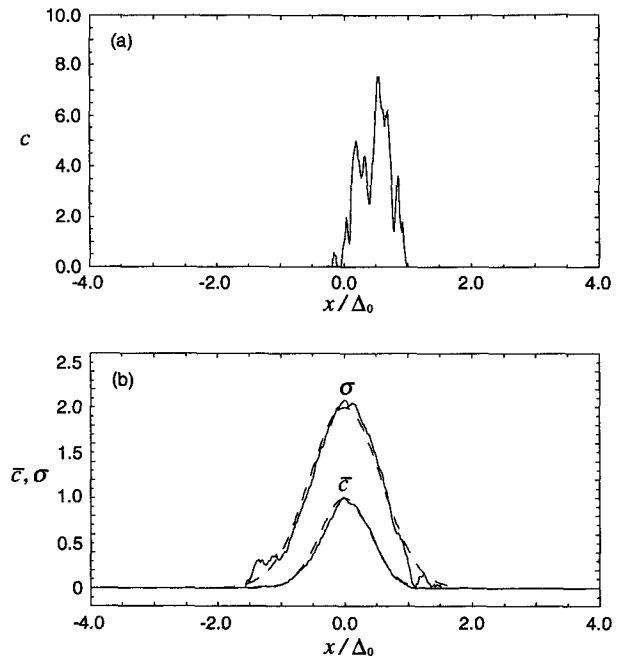

FIG. 9. One-dimensional random pulse fractal generation for an inhomogeneous concentration field with $\sigma_c/\bar{c} = 2$ and local scaling. Solid lines are from fractal generation and dashed lines are the target statistics. (a) Individual realization. (b) Mean $\bar{c}$ and rms fluctuation concentration σ from 1000 realizations.

domize the fractal generation and maintain homogeneity. Lovejoy and Mandelbrot use square pulses with an exponential smoothing factor, but we prefer to use triangular functions to simplify the computation. We adapt the method to the recursive iteration framework by replacing the addition of a random number on the grid of size Δ_n by the addition of an appropriate pulse.

Define the unit triangle function of width Δ at location x_0 as

$$T(x; x_0, \Delta) = \begin{cases} 1 - \dfrac{|x - x_0|}{\Delta}, & |x - x_0| < \Delta \\ 0, & |x - x_0| \geq \Delta. \end{cases} \tag{7}$$

Consider iteration level n at grid size Δ_n with the set of locations

$$\{x_i^{(n)} = (i - 1)\Delta_n, i = 1, M\}.$$

The concentration field is augmented at this level by the addition of the function

$$c^{(n)}(x) = \sum_{i=1}^{M} \epsilon_i^{(n)} T(x; y_i^{(n)}, \Delta_n), \tag{8}$$

where $\epsilon_i^{(n)} \in N(0, \sigma_n)$, that is, a random selection from a normal distribution with zero mean and standard deviation σ_n. Also, the pulse locations $y_i^{(n)}$ are randomly selected from a uniform distribution over the interval $[x_i^{(n)} - \Delta_n/2, x_i^{(n)} + \Delta_n/2]$. The triangular pulse is thus randomized over the appropriate scale and avoids defining any special initial grid. Note that the concentration increment $c^{(n)}(x)$ is a continuous function of x and must therefore be added onto the finest grid. It should be noted that the recursive refinement method is recovered by setting $y_i^{(n)} = x_i^{(n)}$, that is, nonrandom pulse locations.

The variance scaling to obtain σ_0 is more complicated for the triangular pulses since we have to account for the random position of the pulse, but a straightforward integration of the shape function yields

$$\sigma_G^2 = \frac{2}{3}\sigma_0^2 \frac{1 - 2^{-2(N+1)\alpha}}{1 - 2^{-2\alpha}}. \tag{9}$$

The results from the pulse method with $\sigma_c = 2$ are shown in Fig. 7. The ensemble statistics show very good homogeneity and agreement with the analytic prescription. The randomized pulse locations remove the special nature of the initial grid and retain a properly scaled fractal.

The application of the generation technique to represent real plumes must deal with inhomogeneous fields, however, so we next consider a Gaussian concentration distribution. Suppose

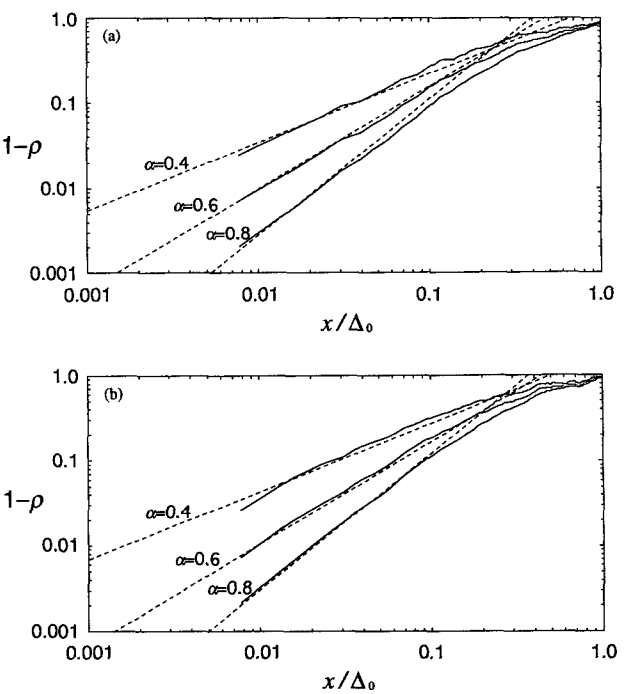

FIG. 10. Correlation coefficient for one-dimensional fractal generation. Solid lines are from the fractal model, and dashed lines are theoretical values (slope is 2α). (a) Homogeneous concentration field. (b) Inhomogeneous concentration field.

Unauthenticated | Downloaded 05/25/22 11:18 PM UTC

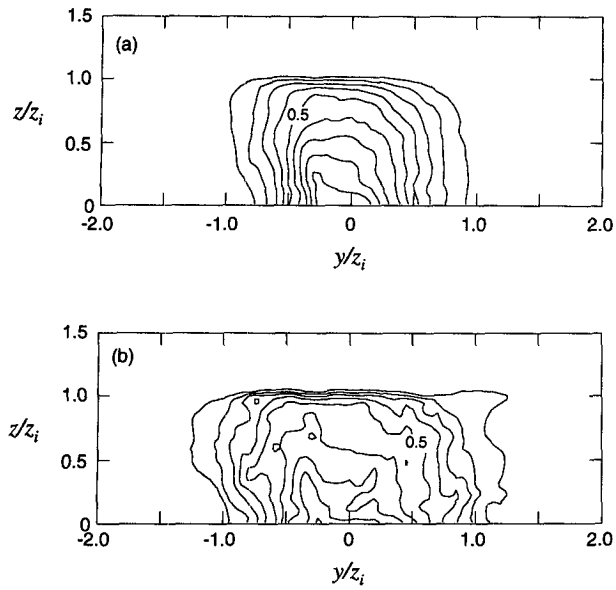

FIG. 11. Transverse cross section of the mean concentration and the rms fluctuation contours for convective boundary layer. Contours normalized by the maximum mean concentration $\bar{c}_m$. Downstream location is at $x/z_i = 8$. (a) Mean concentration; (b) rms fluctuation.

$$\bar{c} = e^{-x^2}$$

$$\overline{c'^2} = \sigma_c^2 e^{-x^2},$$

where the overbar denotes ensemble mean, and the prime denotes fluctuation from the mean. We generate the representation for $x \in [-5, 5]$ and we use $\Delta_0 = 1.25$. This implies a relative large spatial correlation relative to the spread of the distribution but is typical of the LES results.

The first test, shown in Fig. 8, uses the value of $\sigma_n^2(x)$ at $x_i^{(n)}$ as the variance for the selection of $\epsilon_i^{(n)}$; that is, the random number is selected on the basis of the variance at the mean centroid of the pulse. As in the homogeneous case, the mean value $\mu_G(x)$ is used as the initial concentration field to maintain the correct ensemble mean. The use of the local value causes difficulties, however, as seen in the figure. The relative large correlation scale distorts the tails of the distribution. The problem stems from the inaccurate representation of the local statistics by the triangular pulse. With the pulse amplitude determined by the centroid location variance, there is an effective spatial smoothing of the concentration statistics. The nonlinear character of the clipped-normal transformation induces severe distortions in the final results, as seen in the figure.

The predictions for the inhomogeneous case were greatly improved by using a local variance to scale the triangular pulse. Thus, (8) is replaced by

$$c^{(n)}(x) = \sum_{i=1}^{M} \hat{\epsilon}_i^{(n)} \sigma_n(x) T[x; y_i^{(n)}, \Delta_n], \quad (10)$$

where $\hat{\epsilon}_i^{(n)} \in N(0, 1)$. Results using (10) are shown in Fig. 9 for the Gaussian concentration distribution. The agreement with the ensemble statistics is greatly improved.

Spatial correlations are an important characterization of the larger-scale plume fluctuations and will be controlled by our selection of Δ_0, since this represents the maximum range of the correlation. Spatial correlation functions for both a homogeneous fractal and the inhomogeneous Gaussian field are shown in Fig. 10 for several values of α. The correlation is defined at $x = 0$, that is,

$$\rho(x) = \frac{\overline{c'(0)c'(x)}}{[\overline{c'^2(0)}\,\overline{c'^2(x)}]^{1/2}}$$

and shows a similar monotonic decrease for both cases. We actually show $1 - \rho$ on a log–log scale to confirm the power-law behavior for small separations; the correct slope for a fractal field is 2α. As might be expected, the integral scale is smaller for smaller values of α, that is, for higher fractal dimensions, since there is relatively more fluctuation variance in the smaller scales. The point where ρ falls to 0.5 ranges from $0.2\Delta_0$ to $0.4\Delta_0$ as α increases from 0.4 to 0.8. For $\alpha = 0.65$, as used in our fractal field generation in section 4, the corresponding value was roughly $0.33\Delta_0$. This relationship allows us to specify Δ_0 if we are given the correlation scale of the plume fluctuations.

The pulse generation technique is easily extended to higher dimensions by using the product of triangle functions for each separate dimension. The definition of the variance in (9) will contain a 2/3 factor for each

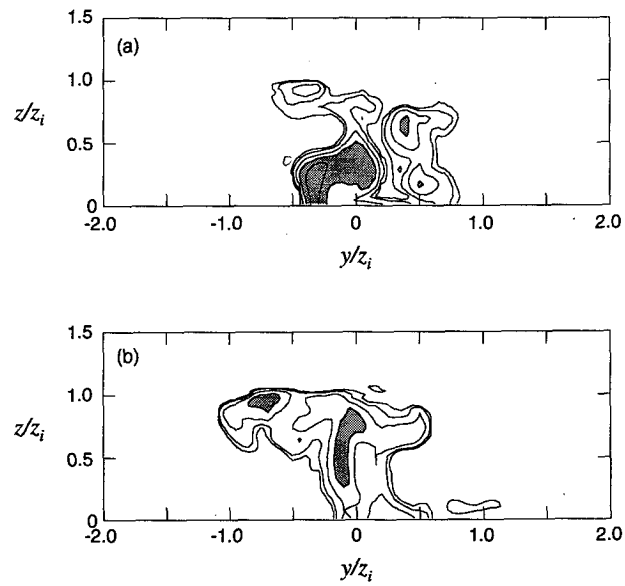

FIG. 12. Two LES convective boundary layer realizations of $c/\bar{c}_m$ at $x/z_i = 8$. Contours at 0.1, 0.2, 0.5, 1, and 2. Stippled areas are equal to or greater than 1.

Unauthenticated | Downloaded 05/25/22 11:18 PM UTC

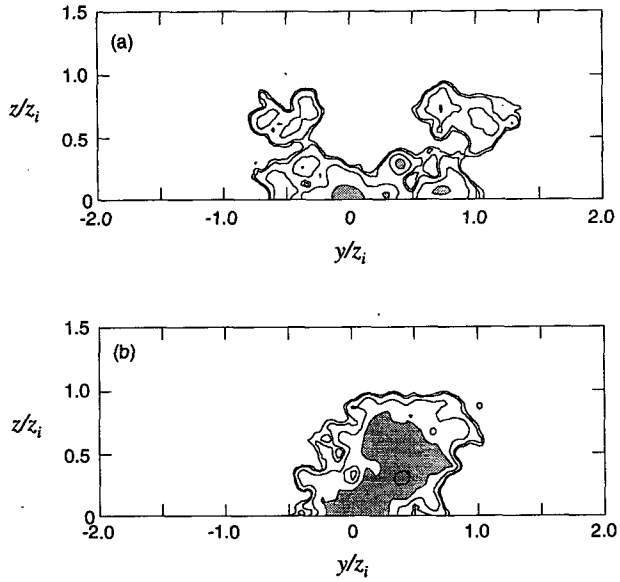

FIG. 13. Two fractal realizations of $c/\bar{c}_m$ at $x/z_i = 8$ using LES convective boundary layer statistics with clipped-normal distribution. Contours at 0.1, 0.2, 0.5, 1, and 2. Stippled areas are equal to or greater than 1.

dimension, but the rest of the methodology is unchanged.

4. Comparison with LES realizations

The fractal generation scheme described in the previous section can be applied to the fields from the LES plume calculations. We first consider the free-convection case at $x/z_i = 8$. This corresponds to a nondimensional distance $X = 2$ downstream, as defined by Henn and Sykes (1992). Here,

$$X = \frac{x}{z_i}\frac{w_*}{U},$$

where z_i is the mixed-layer depth, U is the horizontal translation speed, and w_* is the convective scaling velocity (Deardorff 1970). The mean concentration and the rms fluctuation for the cross section at $x/z_i = 8$ are shown in Fig. 11. The plume is almost completely mixed throughout the depth of the turbulent layer, and the fluctuation intensity, $\sigma_c/\bar{c}$, is roughly 1 in the main part of the plume. The fractal generation also requires a correlation scale to determine the initial grid size Δ_0. The lateral correlation scale, defined as the range at which the correlation coefficient is 0.5, was shown to be roughly $0.25z_i$ at the plume centerline (Henn and Sykes 1992). Thus, using the results from the previous section with $\alpha = 0.65$, we specify $\Delta_0 = 0.75z_i$.

The LES realizations are shown in Fig. 12, while the fractal representations using a clipped-normal distribution are presented in Fig. 13; the lognormal fractal is shown in Fig. 14. The general character of the plume is well represented by the fractal model. The LES resolution is insufficient to check very small-scale fluctuations, but the scale and magnitude of the dominant features match well. The principal difference between the three sets of realizations is evident in the low concentration regions. The clipped-normal representation produces too many zero values compared with the LES, while the lognormal has too few. This is completely consistent with the one-point pdf results from the LES, which showed that the distribution was intermediate between the two idealized shapes.

Box-counting results for the fractally generated convective boundary layer plume are shown in Fig. 15 for both clipped-normal and lognormal distributions. Both plots demonstrate self-similarity over most of the range of scales and are consistent with the fractal analysis of the LES convective plume. The fractal dimension is 1.32 ± 0.05 for the clipped-normal distribution and 1.27 ± 0.05 for the lognormal, compared with the specified dimension of 1.32, as found in the fractal analysis of the LES convective boundary layer plume. The lognormally generated realizations tended to produce a fractal dimension slightly lower than the specified value, and this is attributable to finite resolution and statistical sampling. The dimension is obtained from a relatively low isosurface value, so that a reasonably extensive contour is available, but the probability distribution becomes increasingly intermittent in the edges of the plume and increasingly large samples are required to represent the fluctuations properly. The

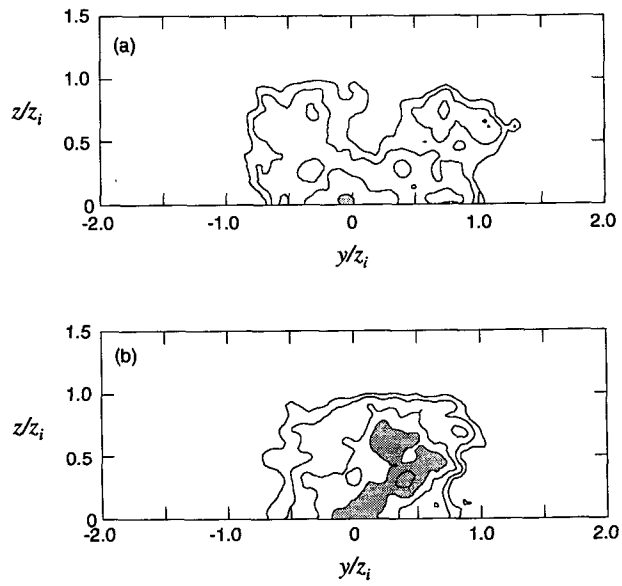

FIG. 14. Two fractal realizations of $c/\bar{c}_m$ at $x/z_i = 8$ using LES convective boundary layer statistics with lognormal distribution. Contours at 0.1, 0.2, 0.5, 1, and 2. Stippled areas are equal to or greater than 1.

Unauthenticated | Downloaded 05/25/22 11:18 PM UTC

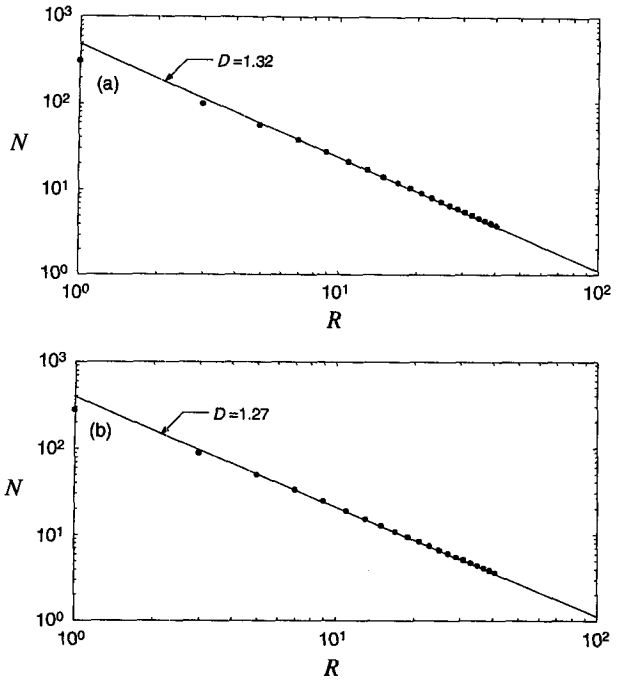

FIG. 15. Box-counting analyses of fractally generated convective boundary-layer plume. (a) Clipped-normal distribution. (b) Lognormal distribution; R is normalized box size and N is the number of boxes.

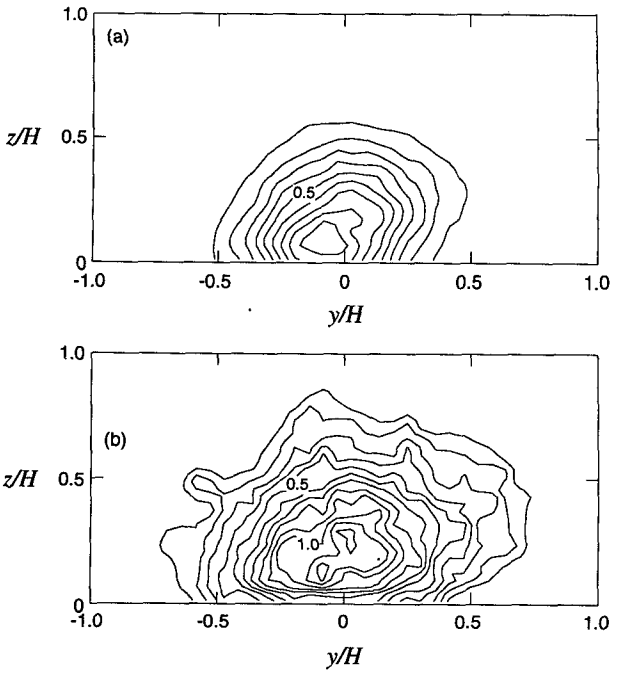

FIG. 16. Transverse cross section of the mean concentration and the rms fluctuation contours for neutral boundary layer. Contours normalized by the maximum mean concentration ($\bar{c}_m$). Downstream location is at $x/H = 5$. (a) Mean concentration; (b) rms fluctuation.

fractal measure was obtained for contour values in the same range as used for the LES data analysis and showed a tendency to reduce as the threshold was reduced. The clipped-normal distribution does not show the same effect, since all small threshold values define the clipped region, which is not strongly dependent on the outer regions of the plume.

Examples of the neutral boundary layer LES plume statistics and realizations are given in Figs. 16 and 17 and can be compared with the fractal plumes in Fig. 18. The lognormal distributions are shown here, since the LES probability density functions (pdf's) were closer to lognormal. The spatial correlation scale was shown to be about $0.09H$ (Sykes and Henn 1992), and we therefore use $\Delta_0 = 0.25H$ in the fractal generation scheme. The fractal technique is not able to reproduce the coherent distortion of the plume that can be seen in the LES realizations, such as the rolled-up feature on the left of Fig. 17b. There is an appropriate spatial length scale for the structures in the fractal field, however, and we have accurately matched the one-point statistics. The one-point pdf is strictly lognormal, due to the addition of independent normally distributed contributions, and we know that this is a good approximation only for the central region of the neutral-layer plume. The distribution in the LES plume edges is more intermittent, as can be seen in the larger region

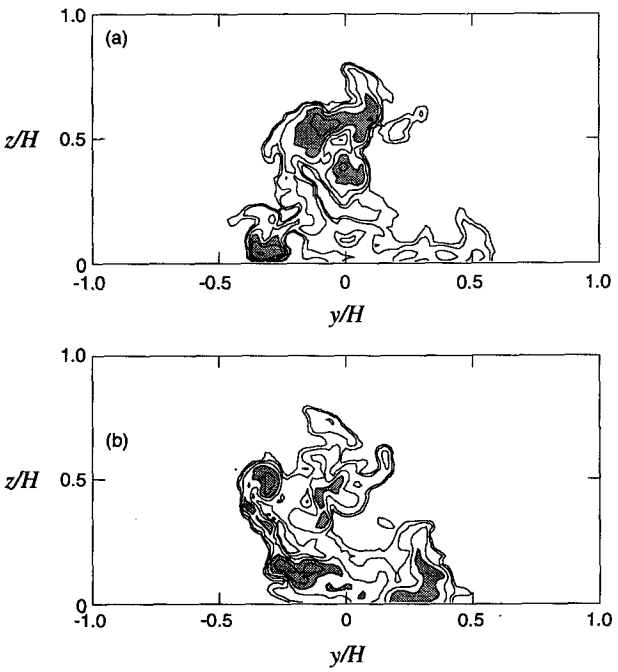

FIG. 17. Two LES neutral boundary layer realizations of $c/\bar{c}_m$ at $x/H = 5$. Contours at 0.1, 0.2, 0.5, 1, 2, and 5. Stippled areas are equal to or greater than 1.

Unauthenticated | Downloaded 05/25/22 11:18 PM UTC

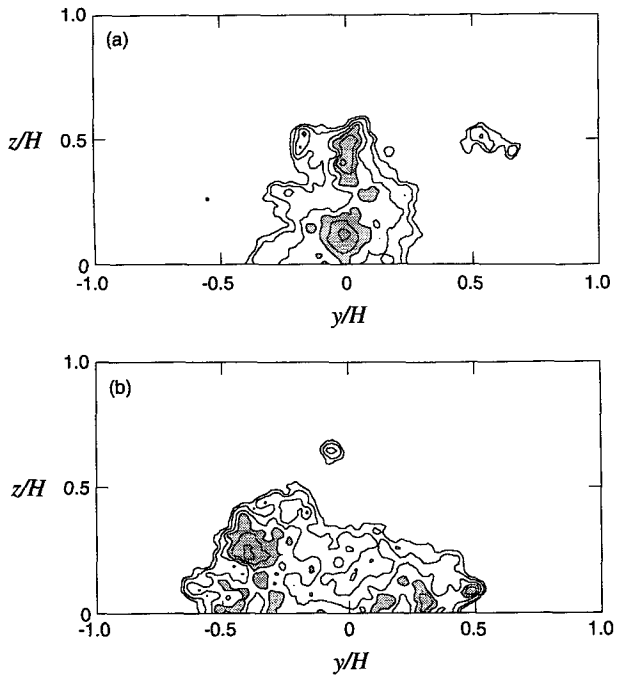

FIG. 18. Two fractal realizations of $c/\bar{c}_m$ at $x/H = 5$ using LES neutral boundary layer statistics with lognormal distribution. Contours at 0.1, 0.2, 0.5, 1, 2, and 5. Stippled areas are equal to or greater than 1.

of low-level concentration in the fractal fields. The LES realization shows regions of "clean" air mixed well into the plume, implying an intermittent pdf. The fractal dimension of the generated "plumes" was 1.30 ± 0.05, somewhat lower than that specified from the LES neutral boundary layer results ($D = 1.36$). The clipped-normal distribution is too intermittent, however, and further work is needed to develop a proper representation of the general probability distribution.

5. Concluding remarks

The LES results of Sykes and Henn (1992) and Henn and Sykes (1992) for turbulent plume dispersion have been used to determine a fractal dimension for the concentration field. Perimeter–area relations and box-counting methods were utilized in the analysis of scalar concentration fields. The dimension of a concentration contour in a two-dimensional cross section was found to be roughly 1.30–1.35 using the two different estimation methods. This is slightly smaller than observational estimates from natural clouds.

The recursive refinement technique has been adapted to provide a consistent representation of the mean and variance of an inhomogeneous concentration field with a clipped-normal or lognormal one-point pdf. The interpolation methodology of the standard method was replaced by a randomized pulse approach to obtain a good match with the ensemble statistics. The fractal generation scheme can be used to generate a concentration field with the desired fractal dimension and accurate ensemble mean moments of first and second order; the scheme also requires the specification of a spatial correlation scale as the outer scale for the fractal field.

The application of the resulting technique using ensemble statistics produced reasonably good "realizations" of the LES plume. The general structure of the plume is reproduced well, although there are differences between the LES pdf's and the idealized shapes. Further work will be needed to generalize the pdf's.

In summary, we have presented a relatively simple fractal generation technique capable of reproducing the mean and variance of an inhomogeneous field in multiple dimensions. The technique can be used in conjunction with parameterized dispersion models such as Sykes et al. (1986), which predict mean and variance of the concentration, to generate quantitatively accurate realizations of an instantaneous field.

Acknowledgments. This work was supported by the U.S. Army Research Office under Contract DAAL03-92-C-0020.

REFERENCES

Cahalan, R. F., and J. H. Joseph, 1989: Fractal statistics of cloud fields. *Mon. Wea. Rev.*, **117**, 261–272.

Csanady, G. T., 1973: *Turbulent Diffusion in the Environment.* Reidel, 248 pp.

Deardorff, J. W., 1970: Convective velocity and temperature scales for the unstable planetary boundary layer and for Rayleigh convection. *J. Atmos. Sci.*, **27**, 1211–1213.

Durbin, P. A., 1980: A stochastic model of two-particle dispersion and concentration fluctuations in homogeneous turbulence. *J. Fluid Mech.*, **100**, 279–302.

Fackrell, J. E., and A. G. Robins, 1982: Concentration fluctuations and fluxes in plumes from a point source in a turbulent boundary layer. *J. Fluid Mech.*, **117**, 1–26.

Feder, J., 1988: *Fractals.* Plenum Press, 283 pp.

Henn, D. S., and R. I. Sykes, 1992: Large-eddy simulation of dispersion in the convective boundary layer. *Atmos. Environ.*, **26A**, 3145–3159.

——, and ——, 1984: Relative diffusion in turbulent media: The fractal dimension of clouds. *Phys. Rev. A*, **29**, 1461–1470.

Kaplan, H., and N. Dinar, 1988: A stochastic model for dispersion and concentration distribution in homogeneous turbulence. *J. Fluid Mech.*, **190**, 121–140.

Lane-Serff, G. F., 1993: Investigation of the fractal structure of jets and plumes. *J. Fluid Mech.*, **249**, 521–534.

Lewellen, W. S., and R. I. Sykes, 1986: Analysis of concentration fluctuations from lidar observations of atmospheric plumes. *J. Climate Appl. Meteor.*, **25**, 1145–1154.

Lovejoy, S., 1982: Area–perimeter relation for rain and cloud areas. *Science*, **216**, 185–187.

——, and B. B. Mandelbrot, 1985: Fractal properties of rain, and a fractal model. *Tellus*, **37A**, 209–232.

——, and D. Schertzer, 1991: Multifractal analysis techniques and the rain and cloud fields from 10^{-1} to 10^{6} m. *Scaling, Fractals and Non-linear Variability in Geophysics.* D. Schertzer and S. Lovejoy, Eds., Kluwer, 111–144.

Malinowski, S. P., and I. Zawadzki, 1993: On the surface of clouds. *J. Atmos. Sci.*, **50**, 5–13.

Unauthenticated | Downloaded 05/25/22 11:18 PM UTC

Mandelbrot, B. B., 1977: *Fractals: Form, Chance and Dimension.* W. H. Freeman, 365 pp.

——, 1982: *The Fractal Geometry of Nature.* W. H. Freeman, 468 pp.

Mylne, K. R., and P. J. Mason, 1991: Concentration fluctuation measurements in a dispersing plume at a range up to 1000 m. *Quart. J. Roy. Meteor. Soc.,* **117,** 177–208.

Peitgen, H.-O., and D. Sauper, 1988: *The Science of Fractal Images.* Springer-Verlag, 312 pp.

Prasad, R. R., C. Menevau, and K. R. Sreenivasan, 1988: Multifractal nature of the dissipation field of passive scalars in fully developed turbulent flows. *Phys. Rev. Lett.,* **61,** 74–77.

——, and K. R. Sreenivasan, 1990a: Quantitative three-dimensional imaging and the structure of passive scalar fields in fully turbulent flows. *J. Fluid Mech.,* **216,** 1–34.

——, and ——, 1990b: The measurement and interpretation of fractal dimensions of surfaces in turbulent flows. *Phys. Fluids A,* **2,** 792–807.

Rys, F. S., and A. Waldvogel, 1986: Fractal shape of hail clouds. *Phys. Rev. Lett.,* **56,** 784–787.

Sawford, B. L., 1987: Conditional concentration statistics for surface plumes in the atmosphere. *Bound.-Layer Meteor.,* **38,** 209–223.

Sreenivasan, K. R., 1991: Fractals and multifractals in fluid turbulence. *Ann. Rev. Fluid Mech.,* **23,** 539–600.

——, and C. Meneveau, 1986: The fractal facets of turbulence. *J. Fluid Mech.,* **173,** 357–386.

Sykes, R. I., and D. S. Henn, 1992: Large-eddy simulation of concentration fluctuations in a dispersing plume. *Atmos. Environ.,* **26A,** 3127–3144.

——, W. S. Lewellen, and S. F. Parker, 1984: A turbulent-transport model for concentration fluctuations and fluxes. *J. Fluid Mech.,* **139,** 193–218.

——, ——, and ——, 1986: A Gaussian plume model of atmospheric dispersion based on second-order closure. *J. Climate Appl. Meteor.,* **25,** 322–331.

Unauthenticated | Downloaded 05/25/22 11:18 PM UTC